THE INJECTOR LINAC FOR THE MAINZ MICROTRON*

H. Euteneuer, H. Braun, H. Herminghaus, R. Klein**, H. Schöler, T. Weis***
Institut für Kernphysik, Universität Mainz, Becherweg 45, D-6500 Mainz, FRG

Summary

The design and setup of a 3.5 MeV, 100 µA injector for a cascade of race track microtrons is presented. It replaces a 2.1 MeV Van de Graaff for getting higher reliability, improved beam dynamics in the first RTM by increased and more stable input energy, as well as an easier access and a better vacuum to launch a beam of polarized electrons. The considerations which led under given boundary conditions to the final design concept are discussed and its realization with PARMELA is described. Details of the linac setup are given. First operation showed a good longitudinal performance (energy stability $\leq \pm 2 * 10^{-4}$, spectrum $\leq 1 * 10^{-3}$ FWHM, bunch length $\leq \pm 1.5°$) and an excellent reproducibility of machine operation.

Indroduction

For the 850 MeV setup of the Mainz Microtron cascade [1] the Van de Graaff preaccelerator injecting into the first race track microtron (RTM) is replaced by a cw rf-linac. The reasons for this change were

a) to get a more reliable and in case of repairs easier accessible injector setup [2]; b) to get the excellent high vacuum necessary for a GaAsP-cathode and the space to launch a beam of polarized electrons [3]; c) to improve the longitudinal stability of RTM1 (14 MeV). With the 2.1 MeV beam from the Van de Graaff a phase migration from +16° at injection to the stable phase angle of -22° [4] occured during the first recirculations of this RTM, resulting in a quite critical longitudinal behaviour. Injection with 3.5 MeV at -12° into the so far third return path of RTM1 will improve this situation very much, just as the fact that d) an rf-linac is insensitive to γ-radiation. Thus the hitherto existing feedback loop, that an increase in γ-radiation level led to erratic quick fluctuations of the Van de Graaff output energy, causing beam losses in the RTM5 with production of even more γ's, will be cut open.

Because a multi-section rf-linac has much more parameters than a simple Van de Graaff, a careful look at the error matrix during design and a diagnostic system as complete as possible are necessary.

Linac Design

Bounds

For our purposes any linac design had to obey more or less strictly the following boundary conditions:

a) rf-power to be delivered by one TH-2075 MAMI standard klystron; b) total length from gun to output end ≤ 10 m, given by the dimensions of the RTM1 + RTM2 (180 MeV) setup; c) on-axis coupled structures of the standard MAMI type, i.e. accelerating gradients ≤ 1.2 MV/m [5]; d) maximum length of one rf-section ≤ 2 m, limited by our vacuum brazing facility; e) input energy ≤ 120 keV ($\beta \leq 0.59$) for an easily accessible air insulated DC-gun; f) output energy (2.1), 2.8 or 3.5 (!) MeV, according to the first three return energies of RTM1; g) no parameter changes for an output current from 0 to 100 µA and h) phase acceptance ±20° for not too strict demands to the chopper system [6].

Possible Configurations

Three paths to realize the MAMI injector were investigated: the first [7] consisted of a rather long graded-β section (1 m, 0.8 MeV) followed by two standard sections ($\beta = 1$). This design was abandoned, because to avoid an excessive phase slip in the $\beta = 1$-sections, they had to be rather short, which resulted in a too high rf-power consumption. An even longer graded-β section - which is difficult to tune and to fabricate - would have overcompensated the advantage of using standard sections for the rest of the linac.

The second path [7] went to the other side in some respect, taking a short graded-β section (0.5 m, 0.25 MeV) and three profiles with $\beta \neq 1$ and an overall length of 5 m, which led to a moderate power consumption. The electron bunch was quite linearly transformed, its final shape being determined along the whole linac. The advantage of this design was its great flexibility to produce a wide range of longitudinal phase spaces at the output, the disadvantage its unacceptable sensitivity to parameter deviations (e.g. a $\Delta\varphi = \pm 1°$ of the last section caused a $\Delta T = \pm 5$ keV in output energy).

The third way, which we realized, is in short the following: sacrificing the linear bunch transformation, the longitudinal phase space is essentially ready formed at the end of the graded-β section. The rest of the linac acts just as an energy booster, transporting the short bunch nearly distortion free with maximum rf-power utilisation at the peak of the accelerating field (i.e. the β of the rf-profile has to be changed, when the phase slip exceeds ~10°; naturally as seldom as possible). This is essentially the NBS-LANL design [8]. We had to investigate, if it works at much lower accelerating gradients and an early transition from graded- to constant-β structure profiles.

Realisation

By this concept and the bounds given above, the design of the MAMI injector was largely determined. It is presented in Fig. 1, as worked out in detail [9,10] with PARMELA. Changes to the program were only done by incorporating new Fourier coefficients for the spatial harmonics of the on-axis field, which we measured on our rf-structure [11,12]. They were of influence for energies < 1 MeV (subroutine CELL), beyond that value the quicker global TANK-routine was used. A design of a transverse optics is quite cumbersome with PARMELA, it was therefore aided by a program solving the envelope equation including space charge [9]. A constraint was, that no focusing elements were permitted to be put over the accelerating structures.

The bunch of length of ±20° from the chopper system is compressed by the prebuncher to ±0.8°, ±1.6 keV (convergent, time-like PARMELA convention) at the entrance of the graded-β section (SE 1). In it the synchronous phase decreases from -18° to -7°, the strong transverse defocusing forces by the rf can just be compensated by two lenses located directly at the ends of this section. The bunch is rotated by just 180° and leaves SE1 again convergent with ±2°, ±1.8 keV at 550 keV. In the booster sections SE2 ($\beta_A = 0.918$, $\beta_B = 0.966$) and SE3 ($\beta = 0.987$) the bunch slips from -14° through +4° to -12°, from -10° through +8° to -8° and from -5° through +5° to -4° up to energies of 1027, 1991 and 3464 keV respectively. Transversally one therefore has a DFFD-focusing scheme. The drift lengths in the chopper-prebuncher-system and from SE1 to SE2 are of influence on the longitudinal beam dynamics

* Work supported by HBFG and DFG, SFB 201.
** Now Dornier Systems, Friedrichshafen, FRG.
*** Institut für Angewandte Physik, Universität Frankfurt.

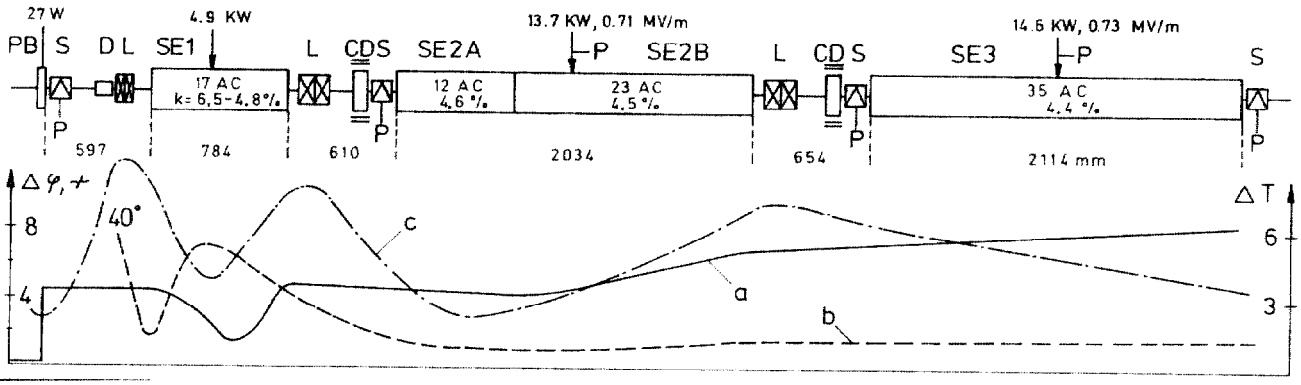

Fig. 1: Scheme of MAMI injector linac with longitudinal and transverse beam envelopes.
PB-Prebuncher, S-Wire Scanner, D-Steering Coils (hor. + vert.), L-Lens, AC-Accelerating Cell, CD-Monitor Cavity + Steering Coils, P-Vacuum Pump. Envelopes: a-ΔT(keV), b-Δφ(degree), c-Radius r (0.1mm).
For gun-chopper-system cf. [6].

the others are quite uncritical. The influence of space charge was investigated for the design current of 100 μA, it enhances the longitudinal and transverse beam envelopes by at maximum a factor of two, mainly in the region of SE1, but had no consequences for the linac design.

The longitudinal error matrix of the linac is visualized in Fig. 2. The numbers indicate, where the center of the output phase space is shifted by certain parameter deviations, its size and shape do not change too much (underlined numbers: starting point is already mistuned linac, here rf-amplitude respectively +1% in SE1 and -1%, +1% in SE2 and SE3 (plus phase compensations), for output energy and phase unchanged). From the "envelopes" d and e one can see, that there is an ample margin to the acceptance ellipse of RTM1.

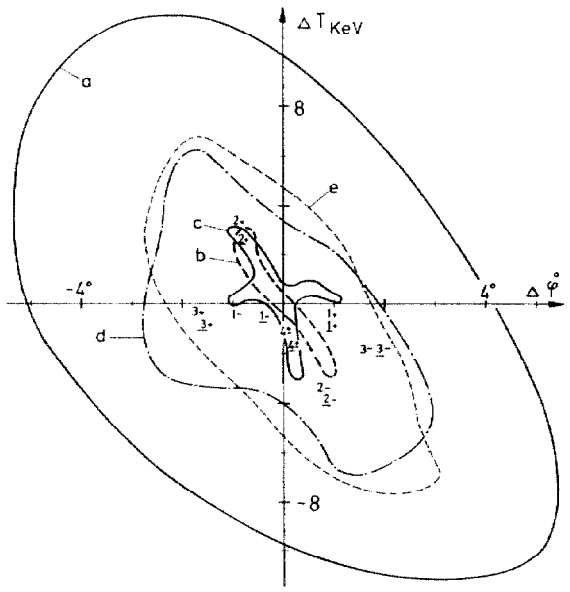

Fig. 2: Longitudinal acceptance of RTM1 (a, divergent)and output of linac (b-without, c-with space charge (100 μA)). Numbers indicate shift of curve c by: 1-Gun ±100 eV, 2-rf-amplitude ±0.1%, 3-SE1 ±1°, 4-SE2 and SE3 ±2°; d-envelope of all this. 1 etc. and curve e - the same, but starting with wrong amplitudes in rf-sections.

Linac Setup

Gun, Chopper, Prebuncher

The gun-chopper-system is presented in detail elsewhere on this conference [6]. The gun has an emittance of 0.6 $\pi * m_o c * mm * mrad$ at 100 μA. Its maximum voltage of 120 kV would have been preferred for an uncritical transverse optics in SE1, for an easier bunch rotation however (and greater safety) 100 kV were taken. The maximum possible chopping ratio (limited by emittance growth) turned out to be a factor of two better than the 1:9 assumed in the linac design.

The prebuncher [18] is a TM_{010}-Al-cavity with a simplified CRNL-β = 0.55 profile, its nominal amplitude is 4.8 keV. A phase stability ≤ 1° (to avoid energy shifts of the beam > 0.1 keV) would demand its temperature control to better than 0.15 °C (Q = 5300), therefore phase control by a tuning plunger was preferred.

Accelerating Structures

The accelerating sections (2450 MHz) were fabricated along the well practized MAMI-technology [5], the only differences being a change in profile of the accelerating cells and in position of the two tuning plungers.

The change in profile was a thinner web (2.9 mm) and a smaller beam hole (12.4 mm) The reasons for this were: a) less change in resonance frequency of the AC's with cavity length at low β for more ease of fabrication of a graded-β section (thinner web, [11]); b) a higher shunt impedance. The TH-2075 is a 50 kW-tube, but for losses in the complicated waveguide system, unforeseen lower quality factors in fabrication of the rf-sections and mainly for regulation of the field amplitude to better 10^{-3} by the rf input power quite far from saturation of the klystron, we set 35 kW as design limit for the rf-power consumption of the linac. The shunt impedance we got is r = 77 MΩ/m, 15% higher than the MAMI value (as a function of β it can be approximated by r = -22.4+102.9*β(MΩ/m), [11]).

The main data for these structures are (β ≥ 0.9, i.e. SE2 and SE3): quality factor 16500; change of passband gap with power -34kHz/kW/m; permanent change of gap during first high power operation +370 kHz (P ≤ 11 kW/m). The passband gap is within ±300 kHz, the nominal resonant frequency was hit by ± 60 kHz. The change of frequency with power is given by

$$\Delta f/kHz = -4.1 * P * (7.2/D + 10.2/D^{1.2} + 1.0/P^{0.4})$$

(P/kW - input power in a 2m-section, D/l/min - water flow; first term in formula: average water warm up, second: temperature jump at water - copper boundary, third: average warm up and elastic deformations of copper).

The two tuning plungers (range 0.85 MHz for SE1, 0.35 MHz for SE2,3) were shifted from the section ends (optimum position for vacuum pumping [5]) to the middle between rf-coupling port and end cavity to have minimum influence of their position on field flatness and relative cavity phase (±2% and ±1.5° are tolerable according to PARMELA calculations). This higher field stability is supported by an 10% increase in coupling constant k (Fig. 1), resulting from the thinner cavity webs.

To give the principal setup of the rf-structures, the graded-β section is shown in Fig. 3. The rf-sections have a pumping port at their vacuum window to trigger an rf-power trip if the pressure exceeds 10^{-3}Pa.

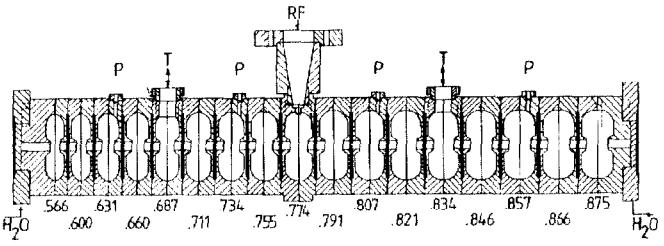

Fig. 3: Graded-β section with β's of cavities (P-Probe, T-Tuner).

RF-System

The 5 couplers and 6 attenuators/phase shifters in the waveguide system feeding the rf-power from the klystron to the cavities were built in circular magic tee technique [13]. The isolation of 33 ±4 dB of these devices turned out not to be high enough to prevent noticeable couplings between different output ports. This affects however only the operational simplicity, not the function of the system.

The central E-field is held constant to better $\pm 2*10^{-4}$ in amplitude and ±0.5° in phase (down from values of $\pm 5*10^{-3}$ and ±5° resulting from a high voltage ripple of $\pm 2*10^{-3}$) via the input power and phase of the klystron. Being away from klystron saturation thus about 20% in efficiency are lost, but with respect to applications in the RTMS, where beam loadings up to 40% are to be compensated, we went away from a HV-regulation [13].

Focusing

The lenses on the linac (Fig. 1) were built as solenoids [17], arranged in counterpoled pairs to avoid rotation of the image plane of the beam and the polarization of electrons. On the injection path from linac to RTM1 (Fig. 4) quadrupoles made from punched Hyperm sheets for a low remanent field (< 0.1 Gauss) are used [17]. The whole linac is magnetically shielded by at least one sheet of 1.5 mm Hyperm .

Steering and Diagnostic

The control hardware for the linac are a Micro VAX II (also to be used for steering the RTMS) and a CAMAC-system crate configuration. The various processes for the accelerator control communicate via the MAMI message system [14].

For longitudinal diagnostics within the linac two TM_{010}-monitor-cavities (Fig. 1), measuring bunch phase and beam current are installed. Together with PARMELA time-of-flight calculations they can also be used for beam energy measurements. A quick diagnostic unit behind the linac is described in [15]. On the injection path to RTM1 a two-wire scanner is installed at the 190°-bend to measure the injection-radius of the beam and thus determine the linac output energy on line [17].

For transverse diagnostics a V-shaped wire setup drawn through the beam measures its horizontal and vertical width simultanously. The variation of beam width as a function of the focal length of a lens, positioned a certain distance in front of such a scanner, is used to determine the transverse phase space ellipses [16].

Injection into RTM1

The scheme is given in Fig. 4. The two end magnets of the 14 MeV-RTM and a 5°-dipole inflect the beam. Two quadrupole doublets and two singulets are available for transverse matching [17]. Q1 is used also, Q3 only for the quick diagnostic unit [15].

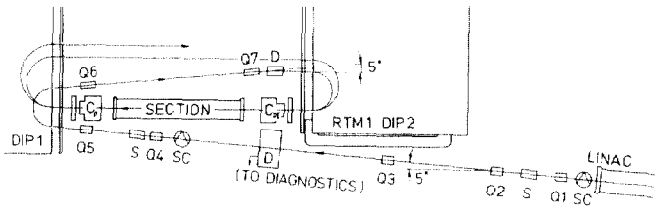

Fig. 4: Injection scheme linac to RTM1 (D-Dipole, Q-Quadrupole, S-Beam Steerer, SC-Scanner, C-Monitor Cavity for phase and intensity).

First Operational Experience

It took only two weeks from first switch-on to remove the severest bugs and to launch a 3.5 MeV beam. The reproducibility of machine operation via computer data bank records was excellent from the beginning. The longitudinal phase space data measured till now are a spectrum FWHM of $9*10^{-4}$(base width $2*10^{-3}$), an estimated bunch length of $\leq \pm 1.5°$ and an energy stability of $\leq \pm 2*10^{-4}$. A detailed verification of the longitudinal error matrix is under way, as well as an analysis of transverse optics. First injection into the 14 MeV-RTM is planned before the end of this year.

References

[1] H. Herminghaus, "Continous Beam Electron Acc.", this conf.
[2] K.H. Kaiser et al., "Four Years of Operation of the 183MeV CW Electron Accelerator MAMI A", this conf.
[3] W. Hartmann et al., "Source of Polarized Electrons", this conf.
[4] H. Herminghaus et al., NIM 138 (1976) 1
[5] H. Euteneuer, H. Schöler, Proc. Conf. LINAC 86, SLAC-Rep.-303
[6] H. Braun, H. Herminghaus, "The Chopper System for the Mainz Microtron", this conf.
[7] R. Klein, Int. Report MAMI 10/83, Inst. f. Kernphysik, Univ. Mainz
[8] M.A. Wilson et al., IEEE Trans. Nucl. Sci., NS-30(1983)3021
[9] T. Weis, Int. Reports MAMI 11/84 and 12/84
[10] H. Euteneuer, Int. Report MAMI 7/85
[11] H. Euteneuer, Int. Report MAMI 9/84
[12] R. Klein, Int. Report MAMI 2/85
[13] H. Herminghaus et al., IEEE Trans. Nucl. Sci. NS-30 (1983) 3274
[14] H.v.d. Schmitt, H. Aufhaus, Proc. LINAC 81, LASL, LA-9234-C
[15] H. Euteneuer et al., "Fast Longitudinal Phase Space Diagnostics for the MAMI B Injector", this conf.
[16] H. Aufhaus, Thesis, Mainz KPH 35/81
[17] Institut für Kernphysik, Univ. Mainz, Jahresbericht 1986/87
[18] H. Euteneuer, H. Schöler, Int. Report MAMI 9/86